

# A Framework for Calibration of Electromagnetic Surgical Navigation Systems

Xiaohui Wu, Russell H. Taylor

Johns Hopkins University, Baltimore, MD USA 21206  
{wux1, rht}@cs.jhu.edu

## Abstract

In this paper, we present a framework of calibrating an electromagnetic tracker (Northern Digital's Aurora) using an accurate optical tracker (the Optotrak system, also from Northern Digital). First, registration methods for these two navigation systems are developed. Sub millimeter accuracy registration is achieved for both cases. We also address the latency between the two different trackers. The registration accuracy for dynamic acquired data is greatly improved after we compensate for the tracker latency. In our calibration approach, we sample the measurement field of the Aurora and compute the position and orientation error using the Optotrak measurements and previously computed registration results as "ground truth". Then we approximate the error field using Bernstein Polynomials. Another comparative technique we use is to decompose the error space using KD tree, and then approximate each atomic cell with local interpolation. Experimental results show significant improvement in tracking accuracy for both position and orientation. Finally we discuss our future directions.

## 1. Introduction

3D Surgical navigation, which is essentially tracking the position and orientation of surgical instruments during operation, is an integral component subsystem in image-guided surgery. The spatial information provided by the tracking device, after registered with imaging system, can provide guidance for manipulations such as needle penetration or endoscopes insertion [1].

Mechanical and optical trackers have been used extensively in computer assisted intervention applications. However they can often be cumbersome and obtrusive in clinical environment. Electromagnetic navigation systems, such as Northern Digital's Aurora are becoming increasingly popular in Minimal Invasive Surgery because they are lightweight, inexpensive and they don't have line-of-sight restrictions. The Aurora (Figure 4) consists of a base unit roughly the size of a volleyball and multiple small position sensors (Figure 1). The small size of Aurora's 5 DOF sensors (0.8mm by 8mm) makes them ideal to be built into customized surgical instruments. Pairs of these sensors have also been combined to produce

6 DOF position and orientation sensors (Figure 1 on the right) manufactured by Traxtal Technologies [2]. Magnetic trackers are suitable for clinical applications where fixed landmarks are hard to find, such as needle tracking in spine surgery, needle placement in liver RF ablation, they can also be used for real-time tracking of tumors, catheters and endoscopes [3-5].

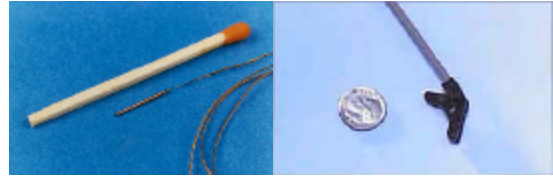


Figure 1. 5DOF sensor (left) and 6DOF sensor (right)

One big disadvantage of almost all electromagnetic trackers is that the measurements can often be degraded by magnetic field distortion caused by environmental metals and electronic equipments. In the past, most magnetic tracker calibration research has been done in the virtual reality research community [6]. Most of the approaches can be divided into two categories: local interpolation [7-12] and polynomial fit [7, 13, 14], local interpolation is faster in computation, whereas polynomial fit have better overall error correction quality [6]. In order to calibrate the measurement distortion of magnetic tracker, a measuring device with high accuracy is usually necessary. In the past, researchers have been using 2D grids on the floor as referencing measurement, however, the data acquisition process can be tedious, and the accuracy could be hard to guarantee. Our method uses a 3D optical navigation system as a reference standard. It is quick and

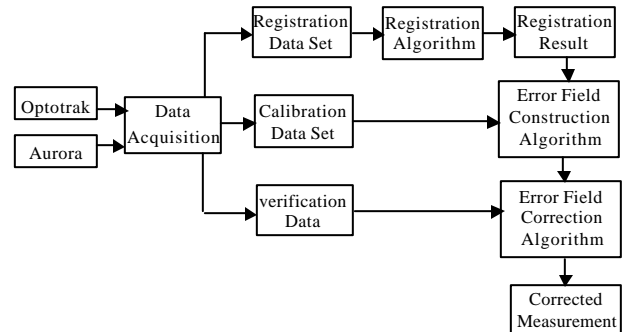


Figure 2. The calibration process

versatile. Further, although we describe it for a particular pair of navigational trackers, it is readily adapted to other 6D measurement systems.

## 2. Approach

### 2.1 Apparatus and calibration process

Our approach uses a specially constructed calibration body to which both Aurora magnetic sensors and infrared light emitting diodes (IREDs) are attached. The 3D positions of the IREDs are measured in real time to an accuracy of 0.1 mm by a Northern Digital Optotrak system. Additional IREDs are attached to the Aurora base, and standard Optotrak utilities are used to associate coordinate systems with IREDs on the calibration body and the Aurora base and to determine the transformation between these coordinate frames. Similarly, the Aurora has standard software both for determining the coordinate transformation of a 6DOF Aurora sensor relative to the base or for determining 3D position and axis direction for a 5DOF sensor. The current paper will focus on calibration using the 6DOF Aurora sensors.

The calibration process (Figure 2) consists of three major steps: a) Optotrak-to-Aurora registration, b) Aurora error field construction and c) error correction and validation. In each step, we acquire multiple samples of data, in which each sample  $k$  consists of  $F_{OT}(k)$ , the transformation of the body IRED coordinate system with respect to the Aurora base IREDS and one or more values  $F_m(i, k)$ , representing the 6DOF position and orientation of the Aurora sensor with respect to the Aurora base:

$$Sample(k) = [F_{OT}(k), F_M(1, k), \dots, F_M(1, N_A)]$$

where  $N_A$  is the number of Aurora sensors on the body.

### 2.2 Calibration body calibration

The purpose of this step is to determine the coordinate transformation between the coordinate system associated with the Aurora sensors on the calibration body and that associated with the IREDs. The coordinate system relationships are shown in Figure 3. Our goal is to determine both a) the transformation,  $F_A^{reg}$ , between the IREDs on the Aurora base and the “base” coordinate system with respect to which the Aurora sensors are measured and b) the transformations  $F_B(i)$  between the body IRED coordinate system and the individual Aurora sensors. The relationship between frames is given by

$$F_A F_m(i, k) = F_{OT}(k) F_B(i) \quad (1)$$

The calibration process is as follows.

**Step 0: Gather data** Acquire samples of data from  $N_p$  different poses of the calibration body.

**Step 1: System simplification.** Define

$$F_C(i, k) = F_m(i, k) F_m(i, 0)^{-1} \quad (2)$$

$$F_D(k) = F_{OT}(k) F_{OT}(0)^{-1} \quad (3)$$

After simplification, we have

$$F_A F_C(i, k) = F_D(k) F_A \quad (4)$$

We can derive

$$R_D(k) = R_A^{-1} R_C(i, k) R_A \quad (5)$$

**Step 2: Find an initial estimation  $R_A^0$  for  $R_A$ .**

$R_C(k)$  and  $R_D(k)$  can be expressed as:

$$R_D(k) = Rot(\bar{q}(k), \mathbf{j}(k)) \quad (6)$$

$$R_C(k) = Rot(\bar{r}(k), \mathbf{q}(k)) \quad (7)$$

We have

$$\bar{q}(k) = R_A \bar{r}(k) \quad (8)$$

$$\mathbf{j}(k) = \mathbf{q}(k) \quad (9)$$

The constraint in equation (9) provides a way to compute the weighting coefficients for  $\bar{q}(k)$  and  $\bar{r}(k)$ . i.e.,

$$\bar{q}'(k) = \frac{\bar{q}(k)}{1 + r \left[ \frac{\mathbf{j}(k) - \mathbf{q}(k)}{\mathbf{j}(k) + \mathbf{q}(k)} \right]^2} \quad (10)$$

$$\bar{r}'(k) = \frac{\bar{r}(k)}{1 + r \left[ \frac{\mathbf{j}(k) - \mathbf{q}(k)}{\mathbf{j}(k) + \mathbf{q}(k)} \right]^2} \quad (11)$$

where  $r$  is a weighting coefficient that can be tuned for faster convergence, and we have

$$\bar{q}'(k) = R_A \bar{r}'(k) \quad (12)$$

An initial estimation  $R_A^0$  of  $R_A$  can be computed from equation (12) using Horn's quaternion method for point cloud registration [15].

**Step 3: Find accurate value of  $R_A$  by iteration.** From

Combined Aurora-Optotrak Rigid Body

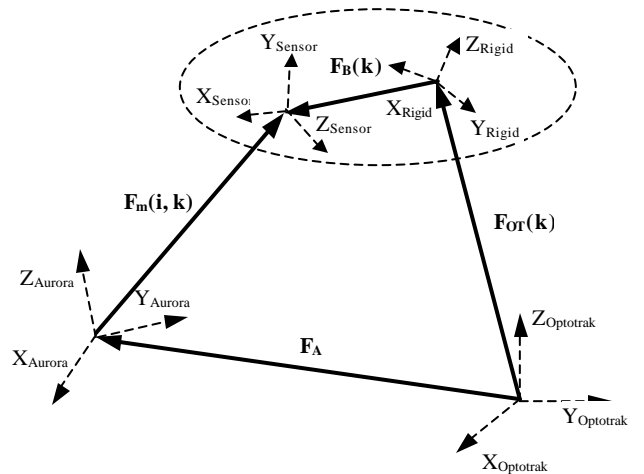


**Figure 3.** Registration of Optotrak and Aurora coordinates

equation (1), we have

$$R_A \bar{P}_B(i, k) + \bar{P}_A = R_D(k) \bar{P}_A + \bar{P}_D(k) \quad (13)$$

Substituting

$$R_A = R_A^{reg} (I - skew(\bar{\mathbf{a}}))$$

into (13) gives

$$(R_D(k) - I) \bar{P}_A + R_A^{reg} skew(\bar{P}_B(i, k)) \bar{\mathbf{a}} = R_A^{reg} \bar{P}_B(i, k) - \bar{P}_D(k) \quad (14)$$

Taking  $R_A^0$  from the previous step as the initial value for  $R_A^{reg}$ , compute  $\bar{P}_A$  and  $\bar{\mathbf{a}}$  using conventional least squares methods. Then update  $R_A^{reg}$  with

$$R_A^{reg} \leftarrow R_A^{reg} Rot_{3c}(\bar{\mathbf{a}}) \quad (15)$$

and iterate until  $\|\mathbf{a}\| < \epsilon$ , a predefined small value.

### Step 3: Compute $F_B(i)$

Rearranging equation (1), we have

$$F_{OT}(k)^{-1} F_A = F_B(i) F_m(i, k)^{-1} \quad (16)$$

Define

$$F_{OT}(k)^{-1} F_A = (R_1(k), \bar{P}_1(k)) \quad (17)$$

and

$$F_m(i, k)^{-1} = (R_2(i, k), \bar{P}_2(i, k)) \quad (18)$$

Then we have

$$\bar{P}_1(k) = F_B(i) \bar{P}_2(i, k) \quad (19)$$

$F_B(i)$  can be estimated using Horn's quaternion point cloud registration method [15].

## 2.3 Aurora Measurement Error Representation

Given a 6D measurement frame from the Aurora

$$F_i = (R_i, \bar{p}_i) \quad (20)$$

where  $R_i$  is the orientation component and  $\bar{p}_i$  is the position vector. The corresponding assumed "ground truth" is

$$F_i^* = (R_i^*, \bar{p}_i^*) \quad (21)$$

We define the error associated with  $F_i$  as

$$E_i = (F_i^*)^{-1} F_i = (R_i^{err}, \bar{\mathbf{e}}_i) \approx (\mathbf{r}_i, \bar{\mathbf{e}}_i) \quad (22)$$

where

$$R_i^{err} = (R_i^*)^{-1} R_i = Rot(\bar{\mathbf{r}}_i, \sin^{-1} \|\bar{\mathbf{r}}_i\|) \quad (23)$$

$$\bar{\mathbf{e}}_i = \bar{p}_i - \bar{p}_i^* \quad (24)$$

Here, the rotation error is represented by a 3D vector  $\bar{\mathbf{r}}_i$ , where the direction and norm of  $\bar{\mathbf{r}}_i$  are the rotation axis and the rotation angle of  $R_i^{err}$  respectively. The advantage this representation is that it is minimal and has no singularities.

## 2.4 KD tree and Local Interpolation

Position error and orientation error can both be expressed as 3D vectors; this enables us to apply the same

error space characterization techniques to both components. In the following discussion, without distinguishing position error and orientation error, we refer to both of them as error vector  $\bar{E}$ .

One way to characterize a multi-dimensional space is to decompose the space into small cells using KD trees. KD tree decomposition is a classical method in computer science. The problem can be described as: given a set of n points in k dimensions contained in a bounding box, hierarchically decompose the bounding box into smaller boxes so that a predefined stopping criterion is met. Stopping criteria can include the number of points in the cell, an approximation residual error threshold etc. The goal is to enhance computation efficiency and reduce the approximation residual. The parameters for the stopping criteria depends on what techniques are used for space approximation, for linear approximation, the KD tree need many levels to achieve the desired performance, as the order of the approximation polynomials increases, the tree can be smaller.

Given an atomic cell defined by its lower bound ( $X_{min}, Y_{min}, Z_{min}$ ) and Upper Bound ( $X_{max}, Y_{max}, Z_{max}$ ), and the cell contains n error vectors  $\bar{E}_{cell}(i) = (e_{x,i}, e_{y,i}, e_{z,i})$  at position  $\bar{v}(i) = (x_i, y_i, z_i)$  for  $i=1$  to n, and we have:

$$\begin{cases} e_{x,i} = c_{00} + c_{01}x_i + c_{02}y_i + c_{03}z_i \\ e_{y,i} = c_{10} + c_{11}x_i + c_{12}y_i + c_{13}z_i \\ e_{z,i} = c_{20} + c_{21}x_i + c_{22}y_i + c_{23}z_i \end{cases} \quad (25)$$

$$\text{or} \quad \bar{E}_{cell}(i) = C_{cell} \bar{V}_i \quad (26)$$

matrix  $C_{cell}$  can be estimated using least squares method. Thus, for position error, with this approximation approach, we first construct a KD tree using the calibration data points, then given an Aurora position vector  $\bar{V}$ , we can search the KD tree to find the atomic cell containing the data point, and compute then error approximation using equation (26), this gives us position error estimation function  $\overline{EP}_{KDT}^N(\bar{V}_i)$ . Similarly we can construct an orientation error approximation function  $\overline{EO}_{KDT}^N(\bar{V}_i)$ .

## 2.5 Error Space Approximation Using Polynomial Fit

Another commonly used technique in approximation is polynomial fit. Suppose we have n calibration data points, for each point  $\bar{V}_i = (x_i, y_i, z_i)$ , the error vector is  $\bar{E}_i = (e_{x,i}, e_{y,i}, e_{z,i})$ , first we compute the normalized coordinates  $(\bar{x}_i, \bar{y}_i, \bar{z}_i)$  for each point,

$$\bar{x}_i = \frac{x_i - x_{min}}{x_{max} - x_{min}} \quad \bar{y}_i = \frac{y_i - y_{min}}{y_{max} - y_{min}} \quad \bar{z}_i = \frac{z_i - z_{min}}{z_{max} - z_{min}} \quad (27)$$

For reasons of numerical stability we use the Bernstein polynomials of degree  $N$  as basis functions.

$$B_{N,k}(x) = \binom{N}{k} (1-x)^{N-k} x^k \quad (28)$$

The goal is to find coefficients  $(N+1)^3$  number of coefficients  $\bar{c}_{jkl}$  satisfying

$$\bar{E}_i(\bar{x}_i, \bar{y}_i, \bar{z}_i) = \sum_{j=0}^N \sum_{k=0}^N \sum_{l=0}^N \bar{c}_{jkl} B_{N,j}(\bar{x}_i) B_{N,k}(\bar{y}_i) B_{N,l}(\bar{z}_i) \quad (29)$$

This is easily done with ordinary least squares methods.

### 3. The Experiment Setup

Data acquisition is a critical step in the tracker calibration process. A good experiment setup should have minimal effects on the tracker electromagnetic field to be calibrated. And because of the large amount of data needed for the registration and error field construction, the data acquisition process should also be relatively efficient.

Our experimental apparatus include a Northern Digital Optotrak 3020, a plastic Lego robot (Figure 4) that can move semi-statically within the desired calibration space and a combined rigid body attached with 6 Optotrak IRED markers and one 6D Aurora dynamic reference body. The Optotrak 3020 is a non-contact optical tracker consisting three CCD cameras and a control unit that interfaces with a PC, it can track the position of IRED markers with RMS error 0.1mm [16].

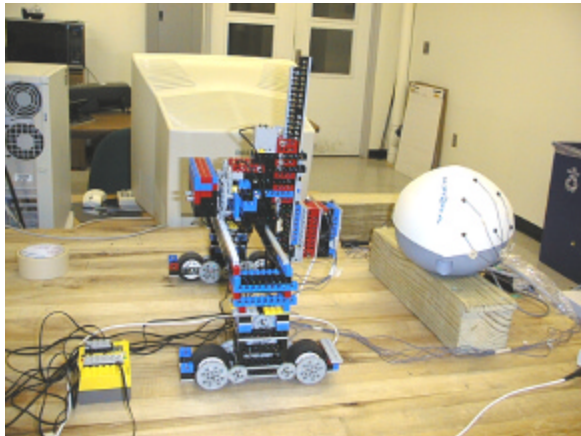


**Figure 4.** Aurora tracker and data acquisition robot

Although 3 IREDs is enough to permit 6D tracking of the calibration body by the Optotrak, we typically use 4-6 IREDs for redundancy. The 6D Aurora dynamic reference body is also rigidly attached to the rigid object. The Lego robot has three DOF translations in  $x$ ,  $y$ ,  $z$  direction. Its sole usage is to place the combined rigid body in close-to-

grid pattern within the working volume of Aurora tracker, thus allow the simultaneous acquisition of Optotrak data and Aurora data.

#### 3.1 Environmental Disturbance Assessment

Potential environmental disturbances include electronic equipment such as the PC, Optotrak and control units for Aurora and Optotrak. Following Northern Digital's guideline, this equipment was kept at least one meter from the Aurora base unit. Another potential source of disturbance was the current used to flash the Optotrak IRED markers during tracking. Experiments showed that when the Aurora sensor closer than 23mm to an IRED marker wire, the induced measurement noise could be as large as 1mm. In our experimental settings, we maintain at least 10mm distance between the Optotrak marker wires and Aurora sensors, and we were able to control the noise to below 0.1mm.

#### 3.2 Dynamic Data Acquisition vs. Semi-static Data Acquisition

The registration and calibration approaches discussed above assume for each sample, data measurements from Aurora and Optotrak correspond to the exact same pose of the calibration body. This is true when the rigid object is static, but it may not necessarily be true when the object is moving. Latency between tracker and reality has been reported before [9], in this case, we are actually interested in the latency between the two different trackers, which has not been characterized by the manufacturer. We did several experiments to study the latency between the two systems. The basic idea is to find the delay that minimizes the registration error developed in our registration process by iterating. Using this protocol, we found the Aurora data constantly lagged behind the Optotrak data for around 80 milliseconds, and this delay was not dependent on the spatial and temporal variation of the movements. A more sophisticated version of this process would actually compute the time delay using standard signal processing techniques, but this was quick and adequate for our purpose. We subsequently automated the process in our registration step.

### 4. Results

#### 4.1 Registration Result

For the registration, we use two methods to acquire data. The first one is placing the combined rigid body at different poses statically, and read from Optotrak and Aurora. Another way is to sweep the rigid body throughout the Aurora measurement volume and read continually from Optotrak and Aurora. The first method is more time-consuming, however, it guarantees that there is

no discrepancy between the Aurora data and Optotrak data. For the dynamically acquired data, we also compared the results of registration with latency compensation and without latency compensation. We evaluate the registration by the average of absolute values of position residual error, which is computed as:

$$\bar{E}_R(k) = F_m(k) \cdot P - \left( (F_A^{reg})^{-1} \bullet F_{OT}(k) \bullet F_B^{reg} \right) \bullet P \quad (30)$$

$$\bar{E}_R = \frac{1}{N_R} \sum_{k=0}^{N_R} |\bar{E}(k)| \quad (31)$$

for each Aurora measurement  $F_m(k)$  and corresponding Optotrak measurement  $F_{OT}(k)$ , where  $F_A^{reg}$  and  $F_B^{reg}(i)$  are registration result for  $F_A$  and  $F_B$  respectively.

**Table 1.** Comparison of registration residual errors for different approaches(in mm)

	x	y	z
$e_D^1$	2.612854	6.623418	4.147685
$e_{DL}^2$	0.514475	0.850873	0.926953
$e_S^3$	0.431387	0.6529	0.83589

<sup>1</sup> $e_D$ : Average residual of dynamic registration w/o latency compensation  
<sup>2</sup> $e_{DL}$ : Average residual of dynamic registration with latency compensation  
<sup>3</sup> $e_S$ : Average residual of static registration

Eight trials were performed for both dynamic registration and static registration. For each dynamic registration, a total of 1000 pose data were gathered. For each static registration trial, a total of 30 pose data were gathered. The results show that our latency compensation approach significantly improves the registration accuracy for dynamically acquired data, the resulting residuals are only slightly worse than the static approach (approximately 0.1mm in each coordinate). This means the data acquisition process can be substantially simplified using dynamic data acquisition.

## 4.2 Calibration Result

We calibrated a cubic volume with side length around 200mm in front of the Aurora field generator. We first collected a calibration data set of size 1500 in the volume. Optotrak data and registration results from section 4.1 are used as “ground truth” to compute both position error vector and orientation error vector for each Aurora measurement as in equation (30), these error vectors are then used to construct the position error estimation function  $\overline{EP}(\vec{v}_i)$  as well as orientation error estimation function  $\overline{EO}(\vec{v}_i)$  using local interpolation in section 2.4 and Bernstein Polynomial fit in section 2.5.

In order to evaluate and compare different calibration methods, we collect a verification data set of 1064 data

points in the calibrated volume. For each measurement frame  $F_i = (R_i, \vec{p}_i)$  we correct the Aurora measurement by using the following equation:

$$F_i^c = (R_i^c, \vec{p}_i^c) = (R_i * Rot(\vec{q}_i, \|\vec{q}_i\|), \vec{p}_i + \vec{d}) \quad (32)$$

where

$$\vec{d}_i = \overline{EP}(\vec{p}_i), \quad \vec{q}_i = \overline{EO}(\vec{p}_i) \quad (33)$$

The Aurora residual error after correction can be computed as

$$F_i^c = (F_i^*)^{-1} F_i^c = (R_i^{err}, \vec{e}_i) \approx (\vec{r}_i, \vec{e}_i) \quad (34)$$

where  $F_i^* = (R_i^*, \vec{p}_i^*)$  is the “ground truth” measurement computed from Optotrak data.

$$F_i^* = \left( (F_A^{reg})^{-1} \bullet F_{OT}(i) \bullet F_B^{reg} \right) \quad (35)$$

**Table 2.** Comparison of Calibration residual errors for different approaches

	Method	Original Error	Corrected error	Improve
Position Error (mm)	A <sup>1</sup>	2.21849	0.331617	85.1%
	B <sup>2</sup>	2.21849	0.230542	89.6%
	C <sup>3</sup>	2.21849	0.191575	91.4%
	D <sup>4</sup>	2.21849	0.190708	91.4%
	E <sup>5</sup>	2.21849	0.236945	89.4%
Orientation Error (degree)	A <sup>1</sup>	0.64190	0.079152	87.4%
	B <sup>2</sup>	0.64190	0.058815	90.8%
	C <sup>3</sup>	0.64190	0.050685	92.1%
	D <sup>4</sup>	0.64190	0.049570	93.3%
	E <sup>5</sup>	0.64190	0.059628	90.7%

<sup>1</sup>Method A: 2<sup>nd</sup> order Bernstein polynomial fit

<sup>2</sup>Method B: 3<sup>rd</sup> order Bernstein polynomial fit

<sup>3</sup>Method C: 4<sup>th</sup> order Bernstein polynomial fit

<sup>4</sup>Method D: 5<sup>th</sup> order Bernstein polynomial fit

<sup>5</sup>Method E: KD tree space decomposition + local linear interpolation

Table 2 shows the average magnitude of position residual error vectors and orientation vectors of the verification data. It can be seen that as the polynomial order increases, the residual errors decrease for polynomial order smaller than 4, as the polynomial order continues to increase, the residual errors hold steady, which basically reflects the static noise level of the Aurora measurements. The KD tree calibration approach has approximately the same performance as the third order Bernstein polynomial fit.

## 5. Conclusion and Future Directions

The experimental results show that the distortion of magnetic trackers can be greatly reduced using our calibration methods. The polynomial fit method yields more accurate results than KD tree local interpolation and gives an efficient closed-form runtime calculation, although it requires more laborious precomputation. The experiments also confirm that the magnetic field distortion can be characterized by fourth order polynomials. We have tested our methods on an Aurora magnetic tracker. However, the approach can be easily extended to other 6DOF sensors.

One important issue in tracker calibration is how to resolve the dependence of tracker error on orientation, which has often been ignored by past research efforts. To fully characterize this dependence, a 6D function will be needed for 6D sensors, which is impractical due to the requirement of large amount of sample data. We are currently working on a new approach to calibrate 5D Aurora raw sensors. By attaching multiple pre-characterized sensors pointing to different directions to the combined rigid body, we can obtain data in multiple orientation by one run of data collection. Thus for a sensor pointing towards arbitrary direction, we can estimate its error vectors by interpolating pre-characterized error spaces corresponding to close by orientation vectors. Our preliminary results indicate that position error can be reduced to within 1mm, and orientation to within 0.5 degrees.

Our experiments were carried out in a controlled, static environment. However, in real clinical scenario, all kinds of disturbance such as electronic equipments, metal devices can be present, meanwhile the environmental disturbance can also be dynamically changing during operation. We are interested in understanding and characterizing the effects of metals and interfering electronics on the measurements of magnetic trackers, especially in developing ways to quantitatively describe these effects by parameters such as polynomial coefficients, KD tree cell size etc.

Further study will also be carried out to facilitate the calibration process and develop clinically compatible surgical instruments with embedded magnetic tracking sensors.

## Acknowledgement

We thank Saibal Chakraborty, Jeff Stanley, Anton Deguet and Anand Viswanathan for providing advice and assistance with the equipments and experiments, we are also thankful for the funding support from Northern Digital Corporation.

## References

[1] F.A. Jolesz, R. Kikinis and F. Shtern, "The Vision of Image-Guided Computerized Surgery: The High-Tech

Operating Room," in *Computer-Integrated Surgery Technology and Clinical Applications*, R. H. Taylor, S. Lavalée, G. C. Burdea and R. Mosges, Ed. Cambridge: The MIT Press, pp. 718-719, 1996.

[2] Traxtal Product Information. <http://www.traxtal.com>

[3] K. R. Cleary, M. Clifford, D. Stoianovici, M. Freedman, S.K. Mun, V. Watson, "Technology improvements for image-guided and minimally invasive spine procedures", *IEEE Transactions on Information Technology in Biomedicine*, Vol. 6 No. 4, pp. 249-261, Dec 2002.

[4] K. R. Cleary, F. Banovac, E. Levy, D. Tanaka, "Development of a liver respiratory motion simulator to investigate magnetic tracking for abdominal interventions", *Proc. SPIE Vol. 4681*, pp. 25-29, 2002.

[5] S. Kirsch, C. Schilling, et al., "Real time tracking of tumor positions for precision irradiation", *Computer Assisted Radiology and Surgery - CAR'98*.

[6] V. V. Kindratenko, "A Survey of Electromagnetic position tracker calibration techniques", *Virtual Reality: Research, Development, and Applications*, vol. 5, no. 3, pp.169-182, 2000.

[7] S. Bryson, "Measurement and Calibration of Static Distortion of Position Data from 3D Trackers", in *Proceedings of SPIE Conference on Stereoscopic Displays and Applications III*, San Jose, CA, pp. 244-255, February 1992.

[8] M. Ghazisaedy, D. Adamczyk, D. Sandin, Kenyon, and T. DeFanti, "Ultrasonic Calibration of a Magnetic Tracker in a Virtual Reality Space", in *Proceedings of the IEEE Virtual Reality Annual International Symposium (VRAIS '95)*, Research Triangle Park, NC, March 1995.

[9] M. A. Livingston, and A. State, "Magnetic Tracker Calibration for Improved Augmented Reality Registration", *PRESENSE: Teleoperators and Virtual Environments*, Vol. 6, No. 5, pp. 532-546, October 1997.

[10] M. Czernuszenko, D. Sandin, T. DeFanti, "Line of Sight Method for Tracker Calibration in Projection-Based VR Systems", in *Proceedings of 2nd International Immersive Projection Technology Workshop*, Ames, Iowa, May 11-12, 1998.

[11] W. Briggs, "Magnetic Calibration by Tetrahedral Interpolation", in *Proceedings of NIST-ASME Industrial Virtual Reality Symposium*, Chicago, IL, MH-Vol. 5/MED-Vol. 9, pp. 27-32, November 1999.

[12] Volodymyr V. Kindratenko, and Angela J. Bennett, "Evaluation of rotation correction techniques for electromagnetic position tracking systems", *Virtual Environments 2000: Proceedings of the Eurographics Workshop*, Springer Computer Science Series, Springer-Verlag, Berlin, Germany, pp. 13-22, 2000.

[13] V. Kindratenko, "Calibration of electromagnetic tracking devices", *Virtual Reality: Research, Development, and Applications*, Vol. 4, pp. 139-150, 1999.

[14] M. Ikits, J.D. Brederson, C. Hansen, and J. Hollerbach "An Improved Calibration Framework for Electromagnetic Tracking Devices", in *IEEE Virtual Reality*, Yokohama, Japan, pp. 63-70, March 13-17, 2001.

[15] B.K.P. Horn, "Closed form solution of absolute orientation using unit quaternions", *J. Opt. Soc. America*, A vol. 4, no. 4, pp 629-642, Apr. 1987.

[16] Northern Digital Product Information. <http://www.ndigital.com>